ACS APPLIED ELECTRONIC MATERIALS

pubs.acs.org/acsaelm

Forum Article

Self-Sustained Quasi-1D Silicon Nanostructures for Thermoelectric Applications

Federico Giulio, Lorenzo Puccio, Stefano Magagna, Alessandro Perego, Antonio Mazzacua, and Dario Narducci*

Cite This: *ACS Appl. Electron. Mater.* 2024, 6, 2917−2924

Read Online

ACCESS | Metrics & More | Article Recommendations | Supporting Information

ABSTRACT: Silicon (Si) nanowires have garnered significant interest for their potential applications in Si-based thermoelectrics, primarily due to their low thermal conductivity. While there are several methods to obtain Si nanowires, their density has been a limiting factor, resulting in a low power density that can be achieved by thermoelectric generators. To address this limitation, metal-assisted chemical etching (MACE) has been developed, enabling the creation of high-density nanopillar "forests". This technique overcomes the previous density constraints. However, Si nanopillars protrude from a bulk Si wafer, which adds its thermal and electric resistivity to those of nanopillars, ultimately reducing the overall power density that can be attained. In this paper, we demonstrate how precise control of pre- and post-MACE processing allows for the creation of fully self-sustained quasi-1D Si nanostructures. We additionally demonstrate that pre-MACE Si processing does not control nanopillar bundling; rather, it primarily determines their shape. This outcome is attributed to the formation of gas nanobubbles during the initial steps of MACE.

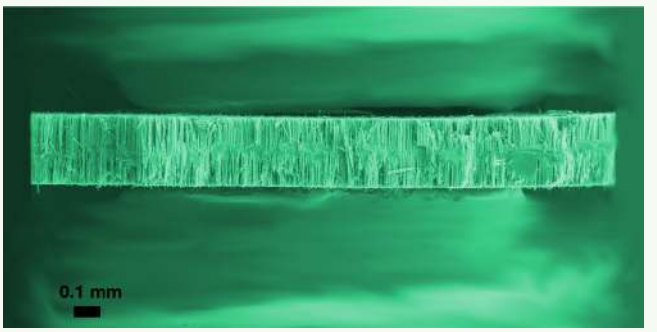

KEYWORDS: *nanowires, nanoridges, silicon, metal-assisted chemical etching, thermoelectricity, nanobubbles*

INTRODUCTION

Crystalline silicon (Si) nanowires (NWs) are a promising option to improve the thermoelectric properties of Si.[1,2] As is known, single-crystalline bulk Si is a poorly performing thermoelectric material.[3] Despite its high power factor (4.5 mW m^{-1} K^{-2} at the optimal doping of 10^{19} cm^{-3}), its high thermal conductivity $\kappa \approx 140$ W m^{-1} K^{-1} at room temperature dramatically reduces its thermoelectric figure of merit to about 0.01 at 300 K.[4] One possible way to reduce κ without affecting the Si Seebeck coefficient α and electrical conductivity σ is through the formation of dimensionally constrained nanostructures (NSs).[1] Si NWs with diameters smaller than the phonon mean-free path reported $\kappa < 5$ W m^{-1} K^{-1}[1,2] due to phonon scattering at NW walls.[5] For the same reason, also Si nanolayers display a lower thermal conductivity, depending on the nanolayer thickness.[6]

Among the techniques that can be used to prepare vertical Si NWs, one-pot metal-assisted chemical etching (MACE) has become very popular because it enables the preparation of high-density NW forests at room temperature and ambient pressure,[7,8] with κ comparable to that of NWs obtained by using extreme lithography.[9] Furthermore, it allows for the formation of NWs of virtually arbitrary length. In a nutshell, one-pot MACE is an etching process based on the local oxidation of Si catalyzed by *in situ*-generated silver (Ag) metallic particles.[10−12] Using a solution containing a Ag salt (e.g., $AgNO_3$) and HF, Ag^+ oxidizes Si while reducing to metallic Ag. Ag nanoparticles act as catalysts for the subsequent Si etching, which preferentially occurs at the Si−Ag interface. Nonetched Si then forms single-crystalline NSs. MACE can be successfully performed on either p- or n-type Si, in a doping range from 10^{15} to 10^{19} cm^{-3}.

In this paper, we confirm that Si NSs obtained by MACE may have a variety of morphologies. NSs obtained under the most common operative conditions are irregularly shaped Si leaves protruding from the wafer surface, with a thickness on the order of 50 nm and a quite variable width, ranging from 100 to 500 nm. We will refer to these as *nanoridges*. Instead, cylindrically shaped Si NWs are obtained when MACE is carried out on pristine oxidized Si. In both cases, the NS shape will be shown to closely depend on the initial step of the MACE process.

An additional leverage to control Si NSs is their agglomeration. Si NS bundling is of paramount relevance in

Special Issue: Advanced Thermoelectric Materials and Devices

Received: July 28, 2023
Revised: September 30, 2023
Accepted: October 2, 2023
Published: October 24, 2023

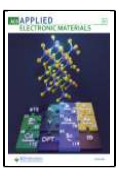

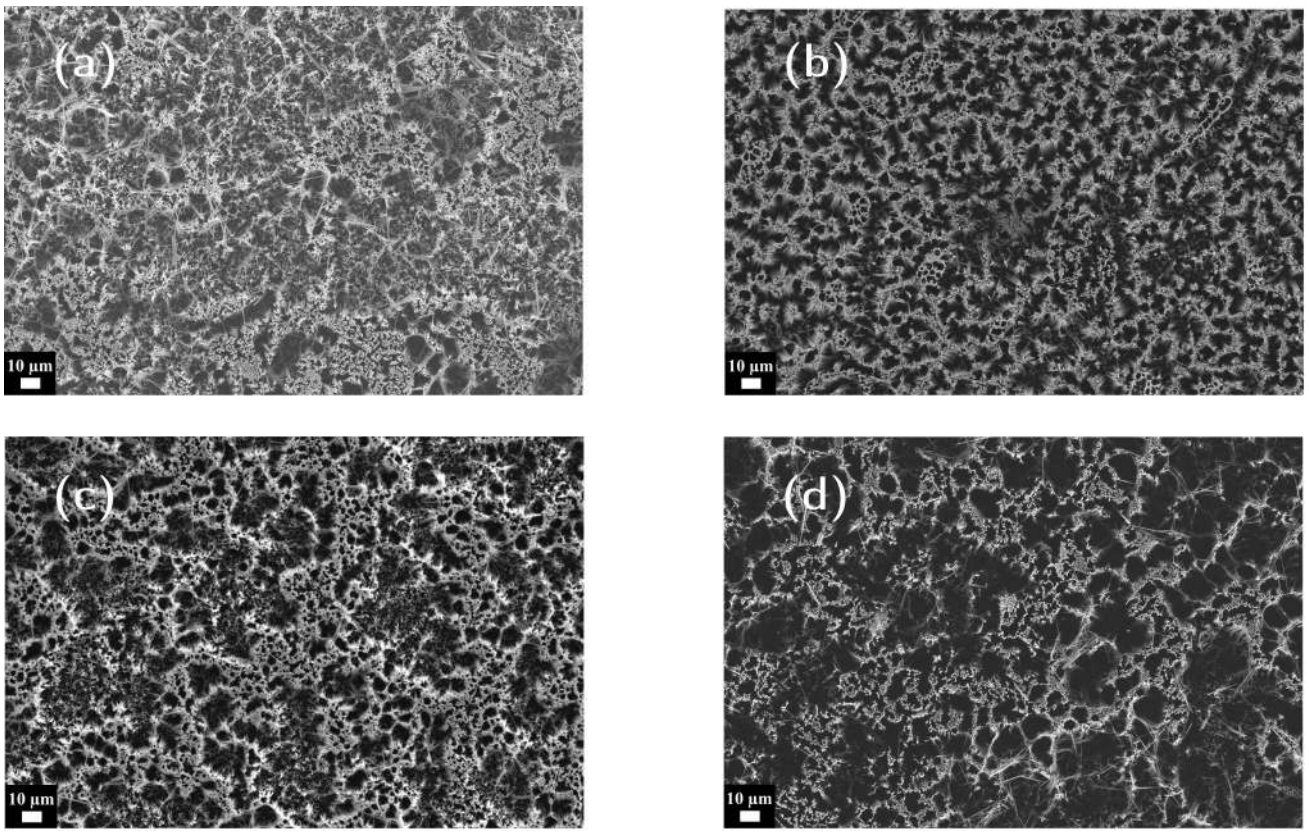

Figure 1. SEM images showing the solvent effect on tip agglomeration on p-type Si NSs. Tip bundling is minimal when drying NSs from acetone (a), being instead comparable when the last solvent is water (b), ethyl acetate (c), or 2-propanol (d). Comparable results are obtained on p^+-type Si (Figure S1).

many applications,[13] from antireflective layers in photovoltaic cells[14] to sensors[15,16] and from electronics[17] to thermoelectric devices.[18,19] Concerning thermoelectrics, tip agglomeration introduces additional electrical contact resistances that are noxious to the device efficiency.[20] Factors affecting tip bundling were then analyzed to either reduce or enhance its extent. We actually found that entangling Si NSs enables the formation of millimeter-sized, self-supporting NS conglomerates that may be used as ordinary legs in the making of thermoelectric devices.

This paper is organized as follows. First, we briefly summarize the literature findings concerning tip agglomeration in Si NSs along with the more puzzling evidence that also the polarity of the pristine wafer surface impacts the density and distribution of Si NSs. On these bases, two sets of experiments are described and commented on, aimed at obtaining tools to control tip agglomeration and at exploring the relationship between the hydrophobicity/hydrophilicity of the initial Si surface and the outcomes of MACE. Evidence confirming the effect of bundling on the NS electrical conductivity and Seebeck coefficient is also presented. Finally, we show how, by making use of both leverages, one may fabricate self-sustaining Si NS conglomerates. An outlook on the use of these novel nanosystems for the development of thermoelectric devices will end the paper.

BACKGROUND

It has been largely reported that, upon MACE termination and following the removal of Ag dendrites, NWs spontaneously tend to agglomerate at their tips, forming bundles.[21,22] Such a feature is mainly caused by capillary forces arising during the drying process. Because, at the end of the process, the removal of Ag dendrites is carried out by using HNO_3, Si NW surfaces oxidize, and water removal (by evaporation) leads to interactions, resulting in tip agglomeration.[23,24] To avoid this, several post-MACE procedures have been advanced. Freezing[25] and supercritical drying[26,27] were found to be very efficient methods. However, they make the entire fabrication process longer and more complicated. Simpler methods were also considered, e.g., using siloxane contact printing.[28]

Both post-MACE steps and the status of the pristine Si surface were reported to affect the NS distribution and density.[20] When MACE proceeded from an oxidized (hydrophilic) Si surface, a higher NS density was observed, with NSs more regularly spaced, and a lower tip agglomeration was reported.[20,22]

While the effect of Si NS termination on agglomeration is quite intuitive, the role played by the termination of the initial Si surface is much less obvious. In most cases, native silicon oxide is removed before MACE by using diluted or buffered HF solutions, leaving a fully hydrophobic surface. When instead either the native oxide or a thicker oxide layer obtained by chemical oxidation is present, exposure of the oxidized surface to the HF-containing MACE solution should rapidly make the surface hydrophobic. Thus, the mechanism linking pristine surface termination to NSs must be associated with the very early stages of MACE.

https://doi.org/10.1021/acsaelm.3c01014
ACS Appl. Electron. Mater. 2024, 6, 2917−2924

EXPERIMENTAL PROCEDURE

Si NSs were prepared starting from [100]-oriented p-type (1−10 Ω cm, [B] = 10^{15} cm^{-3}) and p^+-type (0.01−0.02 Ω cm, [B] = 10^{18} cm^{-3}) single-crystalline Si wafers. Samples were cleaved with a diamond tip to give 10 × 15 mm^2 chips, which were cleaned with dichloromethane, 2-propanol, and deionized (DI) water for 5 min under agitation at room temperature and then dried in a N_2 flux. The final surface was tested to be fully hydrophobic (H-terminated). Samples were then immediately soaked in the MACE solution containing silver nitrate ([$AgNO_3$] = 16 mM) and hydrofluoric acid ([HF] = 5 M). DI water was used throughout the process.

Two different sample sets were prepared. To investigate how chemical processing *after* MACE impacts agglomeration, Si specimens were subjected to MACE for 192 min (set 1). Instead, to study how the hydrophilicity/hydrophobicity of the pristine wafer surface affected the shape and distribution of the NSs, the MACE reaction was ended after 1 min (set 2). Of this second set, an aliquot was oxidized before MACE using ammonium−peroxide mixture solutions[29] [1:1:5 NH_3 (29% vol.):H_2O_2 (33% vol.):H_2O] for 15 min at 65 °C, obtaining a fully hydrophilic surface. The remaining samples were treated instead with a DHF solution (HF 4.4% vol.) to remove the native oxide, obtaining a fully hydrophobic surface. In all cases, MACE was carried out at 20 °C using a thermostatic bath.

At the end of MACE, Ag dendrites were removed using HNO_3 (32% vol.), rinsed with DI water, and subsequently dried in a N_2 flux. Samples from set 1 were then treated with different organic solvents and/or with DHF to quantify the interaction between the NSs and solvent.

The sample morphology was characterized by scanning electron microscopy (SEM) using a Zeiss Gemini 500 scanning electron microscope equipped with a field-emission gun with an acceleration voltage ranging from 0.3 to 30 keV (beam current from 3 pA to 20 nA) and a nominal resolution of 0.6 nm at 15 keV. The instrument was provided with an in-lens detector for both secondary and backscattered electrons, which guaranteed high contrast and resolution.

RESULTS AND DISCUSSION

In this section, we will present and comparatively discuss the effect of the surface hydrophilicity on the distribution and micromorphology (bundling) of the NS forests. It will be confirmed that the bundling is primarily due to the interactions among NS surfaces, and it is then ruled by the final drying process. We present strategies to either enhance or suppress tip agglomeration. Additionally, we show that bundling is fully reversible. Instead, we will provide evidence that the polarity of the pristine Si surface sets the shape of the individual NSs (but not their bundling) as a result of the way Ag nucleates on the wafer surface during the first stages of MACE. Finally, we will show how bundling can be used to obtain self-supporting Si NS conglomerates.

Bundling and Hydrophilicity. As mentioned, it has been largely reported that, during the drying process, NSs may form bundles due to capillary forces, namely, due to the interactions between the NS surface and the last solvent used after Ag removal. Therefore, one expects that tip bundling may be modulated by changing the solvent polarity.[20,30] To verify this hypothesis, samples were soaked in four different solvents—water, 2-propanol, acetone, and ethyl acetate—for 5 min at room temperature and then allowed to dry in air. Figure 1 shows that treatment with acetone is the most effective at preventing tip agglomeration. The NS ends are rather uniformly distributed, and there are large areas where single tips are distinctly visible. Instead, water, 2-propanol, and ethyl acetate are clearly less effective. In-plane tip distribution is much less regular, a confirmation that bundling occurs. This trend is consistent with the electric dipole moment of the solvent molecules (Table 1). When the NS surface is exposed to the solvents, an electrostatic equilibrium is established at the solid/liquid interface[31] that generates an electric field and an electric double layer.[15,32] In the inner Helmholtz layer, molecules are tidily oriented with their positive pole pointing at the oxygen-terminated surface of the NSs. In the diffusion layer, instead, acetone molecules, which have the highest dipole moments, stack more regularly, so that the electrical potential at the interface decays less steeply compared to 2-propanol, ethyl acetate, and water, all sharing similar dipole moments. Thus, acetone more efficiently shields the interaction between the proximal NSs, reducing agglomeration.

Table 1. Electric Dipole Moments of the Solvents Used in This Work

solvent	dipole moment (C m)
acetone	9.0×10^{-30}
water	6.0×10^{-30}
ethyl acetate	5.9×10^{-30}
2-propanol	5.5×10^{-30}

To confirm the role of surface−solvent interactions, an additional set of experiments was carried out, changing the termination of the NS surface by making it H-terminated, etching away the oxide generated by HNO_3. Samples were soaked in a DHF solution for 1 min, then rinsed with DI water, and dried in a N_2 flux to make the surface fully hydrophobic. SEM displays how tip agglomeration is fully prevented, with individual NS tips clearly visible (Figures 2b and S2b). The role of NS surface termination was further checked by drying H-terminated Si NSs out of 2-propanol, acetone, and ethyl acetate (Figures 2 and S2). In no case was tip agglomeration observed because hydrophobic surfaces are not wet by polar solvents.

Because agglomeration depends on the last drying process, one expects that bundling should be reversible, namely, that existing bundled NSs could be separated by making their surfaces hydrophobic, while individual NSs should agglomerate when their surfaces are oxidized. This could be verified by drying NSs out of water, then making the surface hydrophobic by etching it with DHF, and finally reoxidizing it with HNO_3 (Figure 3). At the end of the MACE reaction (terminated by removing Ag dendrites with HNO_3 and using water as the final solvent), NSs bundle as expected. Then, NS surfaces are made hydrophobic by DHF treatment and allowed to dry out of water. Bundles disappear. Finally, when the surface is reoxidized in HNO_3 32% vol. for 15 min, NSs clump together again.

Also the doping level of the NSs plays some role in tip aggregation. In a polar solvent (water), we observed that the higher the doping level, the more evident and stronger the agglomeration (Figure S3) because Si *polarizability* increases with doping.

Pristine Si Surface Hydrophilicity. It was reported[20,33] that NS forest density and distribution also depends on the termination of the pristine Si surface. Evidence was provided that the Si NS density is lower when MACE occurs onto the H-terminated Si surface. Considering that any oxide layer (either native or grown) is obviously removed upon exposure to a HF-containing MACE solution, the impact of the pristine status of the Si chip on the density and distribution of NSs is

https://doi.org/10.1021/acsaelm.3c01014
ACS Appl. Electron. Mater. 2024, 6, 2917−2924

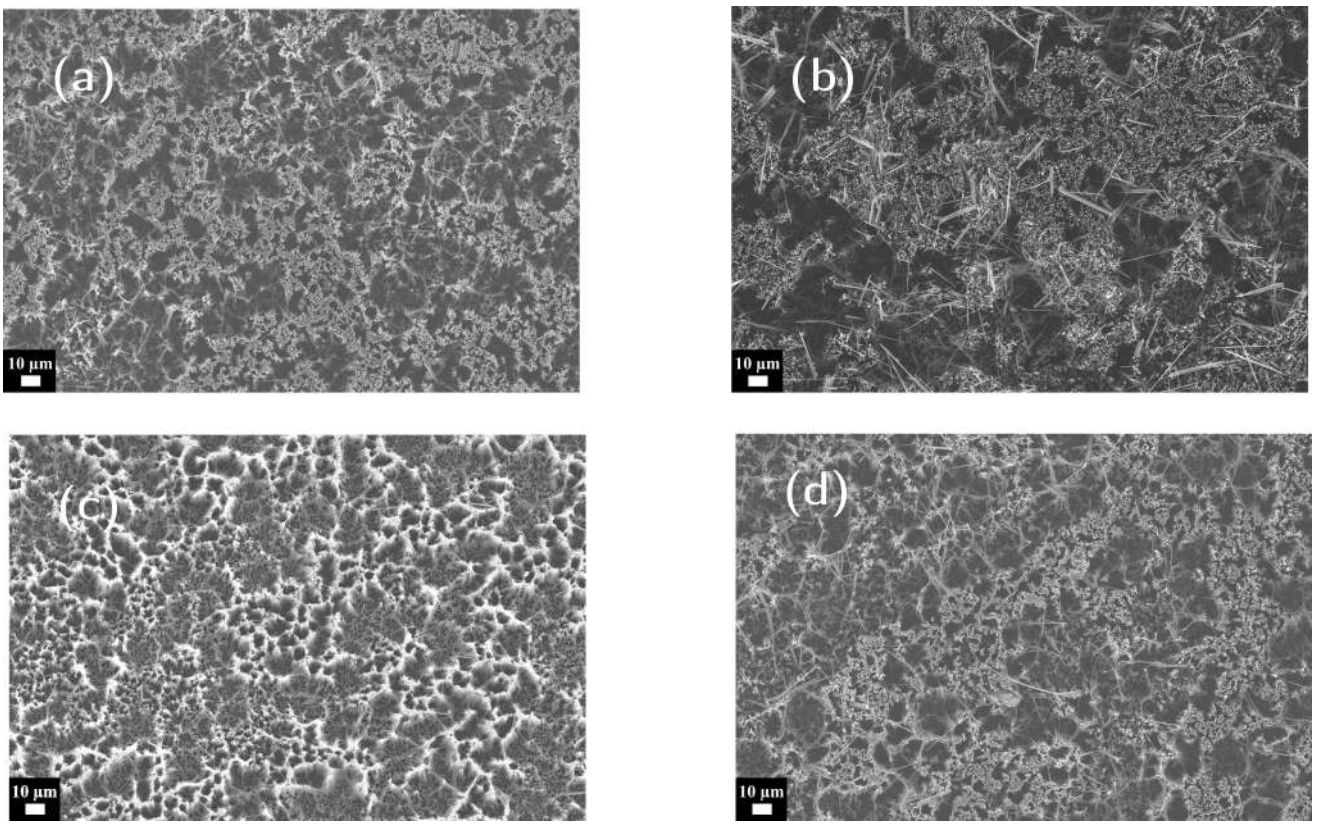

Figure 2. SEM micrographs of Si NSs treated with DHF and then dried out of acetone (a), water (b), ethyl acetate (c), or 2-propanol (d). In all cases tip bundling is minimal, and the effect of the solvent is marginal.

rather puzzling. According to Shiu et al.,[33] a H-terminated pristine Si surface should hinder Ag^+ reduction and, therefore, Ag nucleation. The opposite should happen on the oxidized Si surfaces. As a result, Ag nucleation should occur more uniformly and with a higher density onto Si surfaces that undergo self-limited oxidation by the Piranha etch. Togonal and co-workers[20] explained the trend along the same line, adding that the uniform formation of NWs should also explain the reduced bundling experimentally observed on preoxidized Si surfaces. However, it is known that DHF solutions etch SiO_x at a rate of 23 nm s^{-1} at room temperature.[34] Therefore, even overestimating the thickness of the oxide layer obtained by Piranha to 1 nm,[35] the oxidized surface should be converted by MACE into a fully H-terminated surface after fractions of seconds. Additionally, the possibility that electron exchange may more easily occur through an oxide layer (electrically insulating) compared to a H-terminated surface may be disputable.

To elucidate the underlying mechanism, sample set 2 was prepared by interrupting MACE after 1 min and removing metallic Ag. Etch figures due to Ag reduction are clearly detected. The corresponding final shape of the Si NSs (after full MACE, 192 min) is also displayed in Figure 4. After 1 min from the beginning of MACE, one notes how the distributions of etched regions largely differ depending on the hydrophobicity/hydrophilicity of the wafer surface. We found that oxidized Si displays sparse, isolated, and rounded nuclei. Instead, a hydrophobic Si surface leads to the formation of elongated, continuous Ag aggregates. This suggests that a key role in the initial stage of MACE is played by surface wettability. Upon soaking in the (water-based) MACE solution, a hydrophobic surface, nano- or microbubbles of air dissolved in water are known to steadily form, reducing the contact area of the hydrophobic surface with water.[36] Bubble coalescence then causes the formation of etch-impeded areas, where Ag^+ sorption and reduction may not occur. Because the nanobubble lifetime exceeds 1 min,[37] nucleation of Ag particles may take place only on the portion of the surface in direct contact with the solution. The final result is that Si NSs mirror the distribution of coalesced gas bubbles, leading to the observed formation of *nanoridges*. Instead, when the pristine surface is oxidized, no force stabilizes the nanobubbles. No nanobubble is ever reported to form onto oxidized Si,[36] so Ag nucleation takes places randomly over the whole surface and with a higher density, leading to the formation of Si NWs. Thus, in the former case, *nanoridges* are found. In the latter case, rather Si NWs (either bundled or isolated, depending on the final drying step) are obtained. It must be stressed that nanoridges are *not* tip-agglomerated NWs, although they might have been mistaken as such. As proof, no post-MACE treatment (neither DHF deoxidation or use of polar solvents) leads to changes of the nanoridge shape.

Note that this model is perfectly consistent with Shiu's and Togonal's experimental results of NS density and distribution and with pieces of evidence subsequently reported in the literature by other scholars.[10,22,38]

Modulation of the Thermoelectric Properties of Si NSs. The effect of the formation of Si NSs by MACE on transport properties was the subject of previous publications.[12,39] We showed that, in Si NSs with sizes of >10 nm no change of the Seebeck coefficient occurred because electrons are not quantum-confined. Instead, a remarkable reduction of

https://doi.org/10.1021/acsaelm.3c01014
ACS Appl. Electron. Mater. 2024, 6, 2917−2924

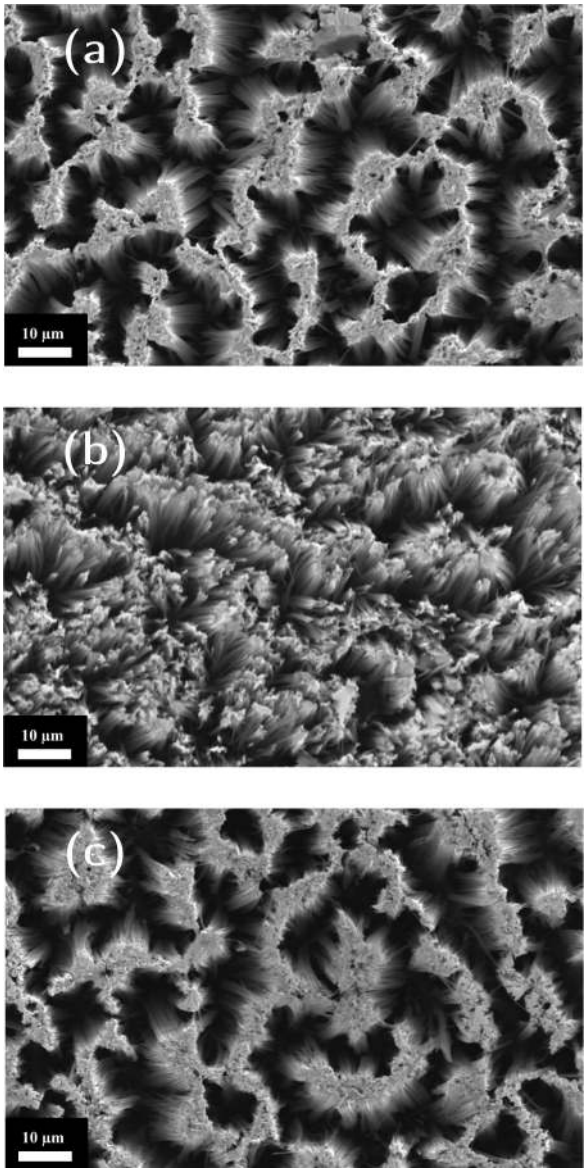

Figure 3. Reversibility of the agglomeration process on a p^+-type sample: (a) oxidized NSs after the MACE reaction; (b) upon treatment with DHF; (c) after reoxidation with HNO_3. All steps were terminated by drying the sample out of water.

the thermal conductivity was observed, down to ≈2 W m^{-1} K^{-1}, with thermal contact resistance marginally affecting the thermal resistance of NS forests. While bundling is then not expected to impact either the Seebeck coefficient or thermal conductivity, its reported effect on the electrical resistance of pillared Si needs to be confirmed. To this aim, contacts were fabricated on bundled and unbundled p^+-type Si NSs (length of 60 μm) by depositing copper (Cu) contacts (contact area of 0.6 cm^2) on Si tips and on the back of the Si substrate.[18] Current−voltage characteristics were measured at room temperature in a two-wire configuration. Bundled and unbundled NSs reported total resistances of $(1.9 \pm 0.3) \times 10^3$ and 89 ± 10 Ω, respectively. Neglecting the possible contact resistance at the back-contacts and because the NS density, width, and length are the same in the two types of NS forests, the change of resistance must be ascribed to contacts at the pillared side. Such a large increase confirms how avoiding tip agglomeration is beneficial to the making of Si NSs for thermoelectric harvesting and is in agreement with previous literature reports.[20] An increase by a factor 20 of the electrical contact resistance may be explained considering that when NSs bundle, Cu cannot conformally cover agglomerated NS tips because agglomerates are exposed to the solution misoriented (randomly oriented) tip ends and electrochemical Cu deposition takes place under strongly irreversible conditions (voltage up to 0.5 V). As a result, Cu initially grows at the sharp edges of tip agglomerates, where the electric field is larger. This brings on the formation of metal blobs[39] that shadow portions of the tip ends, which then remain uncovered by the metal layer. Therefore, the real (microscopic) Si−Cu contact area is largely reduced, causing high contact resistances. Instead, when NSs do not aggregate, the metal may more uniformly cover the NS ends as they are individually exposed to the Cu-containing solution with no shadowing effect.

From NS Forests to Self-Sustained NS Conglomerates. Control over the handles setting the tip agglomeration and NS shape naturally enables further engineering of the system. As shown, unbundled (isolated) NSs enable thermoelectric devices with lower electrical resistances and therefore are capable of larger power densities. However, enhanced tip agglomeration allows for the design of self-sustained NS conglomerates. Because with one-pot MACE there is no limit to the achievable NS length (i.e., to the etching depth), one may continue the etching reaction until the whole bulk Si substrate is etched. Manifestly enough, if NSs were isolated, this would lead to their disaggregation. However, if bundling takes place, then NS conglomerates may be obtained, with NSs sticking together by disorderly joining to each other at their tips. Figure 5 shows such structures, obtained on both n- and p-type Si. We named them *nanofelts* because their mechanical stability is granted by a mechanism closely reminiscent of that of felt fabrics. The absence of a continuous residual Si membrane was verified by permeation tests further than by SEM. Nanofelts reported a good mechanical stability upon the application of hydrostatic pressure (normal to the nanofelt surface) up to 0.5 MPa, fully comparable to supported nanoforests, while they easily break apart upon the application of shear stress. Nonetheless, the possibility of obtaining conglomerates made only of Si NSs discloses quite interesting opportunities, including that of obtaining conventionally shaped thermoelectric legs, establishing a novel route to deploying nanotechnology in macroscopic thermoelectric devices.

SUMMARY AND CONCLUSIONS

It has been shown that several leverages are available to control the agglomeration of Si NSs obtained through one-pot MACE, as summarized in Table 2. We confirmed that the main mechanism leading to the formation of tip bundles is the interaction between the last solvent used after the removal of Ag dendrites. The extent of tip agglomeration may be tailored by changing the solvent polarity and the termination of the NS surface. The latter was found to be the most effective at preventing bundling because the removal of the oxide layer forming on Si NSs upon exposure to nitric solution makes NS surfaces hydrophobic, thus minimizing their electrostatic interactions. We also demonstrated that tip agglomeration is fully reversible. Additionally, we clarified that termination of the pristine Si surface rules the shape of Si NSs obtained by MACE. It is conceivable that the coalescence of gas

https://doi.org/10.1021/acsaelm.3c01014
ACS Appl. Electron. Mater. 2024, 6, 2917−2924

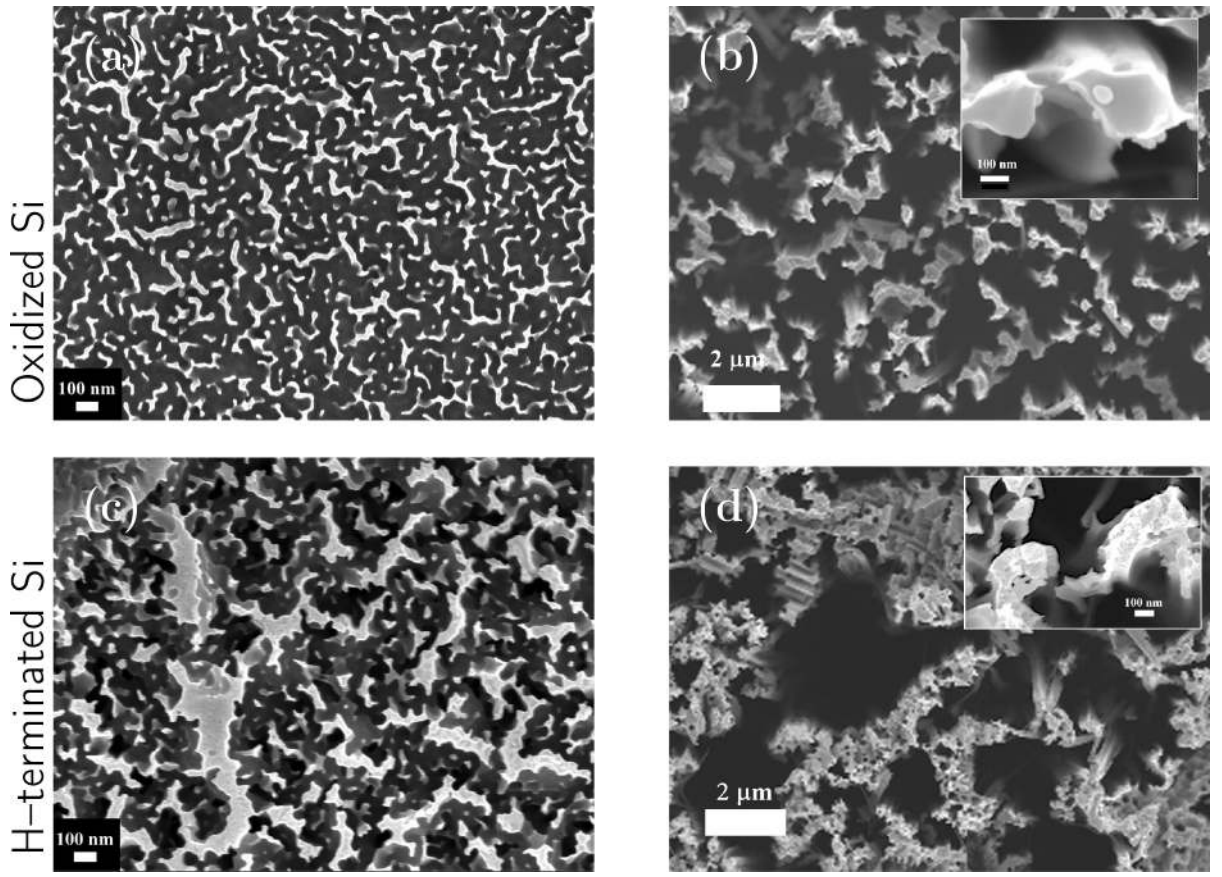

Figure 4. SEM images showing p-type Si surfaces after 1 min of MACE followed by removal of Ag nanoparticles (a and c) and at full completion of MACE (b and d) when MACE is carried out on pristine hydrophilic (oxidized) (a and b) or hydrophobic (H-terminated) (c and d) Si surfaces. The insets display the formation of NWs in the former case and that of nanoridges in the latter case.

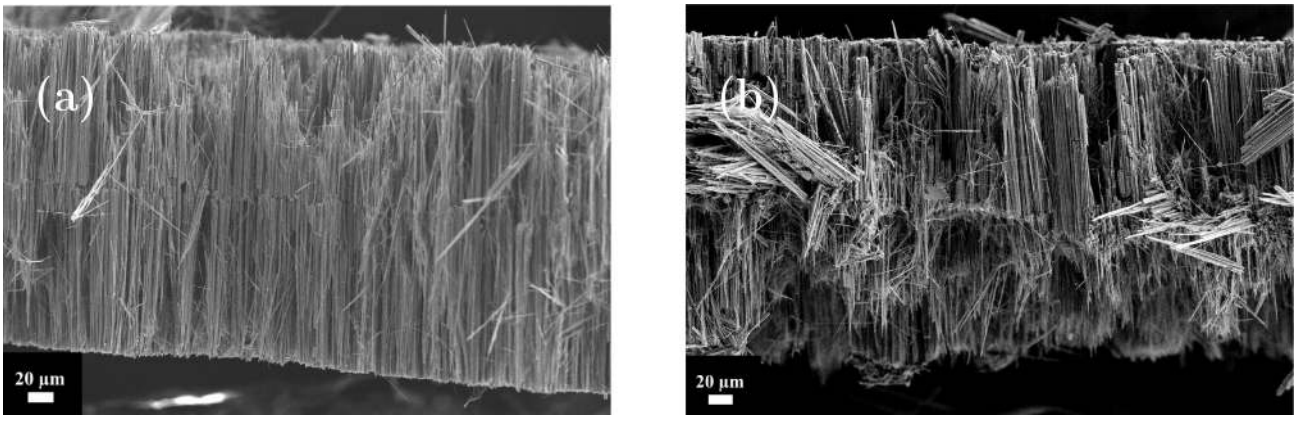

Figure 5. SEM cross-sectional images of (a) p-type and (b) n-type nanofelts obtained through the MACE reaction upon full removal (by MACE) of the Si substrate. Nanofelt thicknesses are ≈0.26 mm.

Table 2. Summary of the Interplay between Chemical Pre/Post-MACE Processing and NS Morphology and Bundling, Remarking How Pristine Wafer Surface Termination Rules the NS Morphology, While NS Termination and Solvent Dipole Moments Control Bundling

			pristine surface	
	NS surface	solvent μ	H-terminated	oxidized
postprocessing	H-terminated	high	nanoridges, unbundled	NWs, unbundled
		low	nanoridges, unbundled	NWs, unbundled
	oxidized	high	nanoridges, almost unbundled	NWs, almost unbundled
		low	nanoridges, bundled	NWs, bundled

https://doi.org/10.1021/acsaelm.3c01014
ACS Appl. Electron. Mater. 2024, 6, 2917−2924

nanobubbles trapped at the Si surface drives MACE to form either NWs or nanoridges. The process is irreversible and, therefore, is not connected with bundling, as suggested in previous publications. Finally, we showed for the first time the possibility of making fully self-sustained NS conglomerates whose stability is granted by the (beneficial) formation of tip aggregates. Additional analyses of the applicability of such novel fascinating structures in thermoelectricity are underway.

■ ASSOCIATED CONTENT

Supporting Information

The Supporting Information is available free of charge at https://pubs.acs.org/doi/10.1021/acsaelm.3c01014.

SEM images of comparative tip bundling upon postprocessing with water and organic solvents in p^+-type samples, higher-resolution SEM micrographs of samples treated with DHF and dried out of water and organic solvents, and SEM top-view images displaying tip bundling dried out of water upon increasing Si doping (PDF)

■ AUTHOR INFORMATION

Corresponding Author

Dario Narducci − *Department of Materials Science, University of Milano−Bicocca, I-20125 Milan, Italy;* orcid.org/0000-0002-3307-1070; Phone: +39 02 64485137; Email: dario.narducci@unimib.it

Authors

Federico Giulio − *Department of Materials Science, University of Milano−Bicocca, I-20125 Milan, Italy*

Lorenzo Puccio − *Department of Materials Science, University of Milano−Bicocca, I-20125 Milan, Italy*

Stefano Magagna − *Department of Materials Science, University of Milano−Bicocca, I-20125 Milan, Italy*

Alessandro Perego − *Department of Materials Science, University of Milano−Bicocca, I-20125 Milan, Italy*

Antonio Mazzacua − *Department of Materials Science, University of Milano−Bicocca, I-20125 Milan, Italy*

Complete contact information is available at: https://pubs.acs.org/10.1021/acsaelm.3c01014

Notes

The authors declare no competing financial interest.

■ ACKNOWLEDGMENTS

F.G. acknowledges the support received by the Ministry of University and Research in the frame of the PON Program "Research & Innovation" 2014−2020, Axis IV, Action IV.5, Grant DOT 13C6492.

■ REFERENCES

(1) Hochbaum, A. I.; Chen, R.; Delgado, R. D.; Liang, W.; Garnett, E. C.; Najarian, M.; Majumdar, A.; Yang, P. Enhanced thermoelectric performance of rough silicon nanowires. *Nature* **2008**, *451*, 163−167.

(2) Boukai, A. I.; Bunimovich, Y.; Tahir-Kheli, J.; Yu, J.-K.; Goddard, W. A., III; Heath, J. R. Silicon nanowires as efficient thermoelectric materials. *Nature* **2008**, *451*, 168−171.

(3) Narducci, D.; Giulio, F. Recent advances on thermoelectric silicon for low-temperature applications. *Materials* **2022**, *15*, 1214.

(4) Glassbrenner, C. J.; Slack, G. A. Thermal Conductivity of Silicon and Germanium from 3 K to the Melting Point. *Phys. Rev.* **1964**, *134*, A1058−A1069.

(5) Lee, S.; Kim, K.; Kang, D.-H.; Meyyappan, M.; Baek, C.-K. Vertical Silicon Nanowire Thermoelectric Modules with Enhanced Thermoelectric Properties. *Nano Lett.* **2019**, *19*, 747−755.

(6) Ju, Y. S.; Goodson, K. E. Phonon scattering in silicon films with thickness of order 100 nm. *Appl. Phys. Lett.* **1999**, *74*, 3005−3007.

(7) Schmidt, V.; Wittemann, J. V.; Gösele, U. Growth, Thermodynamics, and Electrical Properties of Silicon Nanowires. *Chem. Rev.* **2010**, *110*, 361−388.

(8) Huang, Z.; Geyer, N.; Werner, P.; de Boor, J.; Gösele, U. Metal-Assisted Chemical Etching of Silicon: A Review. *Adv. Mater.* **2011**, *23*, 285−308.

(9) Pennelli, G.; Elyamny, S.; Dimaggio, E. Thermal conductivity of silicon nanowire forests. *Nanotechnology* **2018**, *29*, 505402.

(10) Smith, Z. R.; Smith, R. L.; Collins, S. D. Mechanism of nanowire formation in metal assisted chemical etching. *Electrochim. Acta* **2013**, *92*, 139−147.

(11) Srivastava, S. K.; Kumar, D.; Schmitt, S. W.; Sood, K. N.; Christiansen, S. H.; Singh, P. K. Large area fabrication of vertical silicon nanowire arrays by silver-assisted single-step chemical etching and their formation kinetics. *Nanotechnology* **2014**, *25*, 175601.

(12) Magagna, S.; Narducci, D.; Alfonso, C.; Dimaggio, E.; Pennelli, G.; Charaï, A. On the mechanism ruling the morphology of silicon nanowires obtained by one-pot metal-assisted chemical etching. *Nanotechnology* **2020**, *31*, 404002.

(13) Raman, S.; A, R. S.; M, S. Advances in silicon nanowire applications in energy generation, storage, sensing, and electronics: a review. *Nanotechnology* **2023**, *34*, 182001.

(14) Liu, X.; Radfar, B.; Chen, K.; Setälä, O. E.; Pasanen, T. P.; Yli-Koski, M.; Savin, H.; Vähänissi, V. Perspectives on Black Silicon in Semiconductor Manufacturing: Experimental Comparison of Plasma Etching, MACE, and fs-Laser Etching. *IEEE Trans. Semicond. Manufact.* **2022**, *35*, 504−510.

(15) Archer, M.; Christophersen, M.; Fauchet, P. Electrical porous silicon chemical sensor for detection of organic solvents. *Sens. Actuators B: Chem.* **2005**, *106*, 347−357.

(16) Duan, W.; Zhi, H.; Keefe, D. W.; Gao, B.; LeFevre, G. H.; Toor, F. Sensitive and specific detection of estrogens featuring doped silicon nanowire arrays. *ACS Omega* **2022**, *7*, 47341−47348.

(17) Linevych, Y.; Koval, V.; Dusheiko, M.; Yakymenko, Y.; Lakyda, M.; Barbash, V. Silicon Diode Structures Based on Nanowires for Temperature Sensing Application. *2022 IEEE 41st International Conference on Electronics and Nanotechnology (ELNANO)*; IEEE, 2022; pp 190−195.

(18) Dimaggio, E.; Narducci, D.; Pennelli, G. Fabrication of Silicon Nanowire Forests for Thermoelectric Applications by Metal-Assisted Chemical Etching. *J. Mater. Eng. Perform.* **2018**, *27*, 6279−6285.

(19) Dong, J.; Suwardi, A.; Tan, X. Y.; Jia, N.; Saglik, K.; Ji, R.; Wang, X.; Zhu, Q.; Xu, J.; Yan, Q. Challenges and opportunities in low-dimensional thermoelectric nanomaterials. *Mater. Today* **2023**, *66*, 137−157.

(20) Togonal, A. S.; He, L.; Roca i Cabarrocas, P.; Rusli. Effect of Wettability on the Agglomeration of Silicon Nanowire Arrays Fabricated by Metal-Assisted Chemical Etching. *Langmuir* **2014**, *30*, 10290−10298.

(21) Guo, Z.; Jung, J.-Y.; Zhou, K.; Xiao, Y.; won Jee, S.; Moiz, S. A.; Lee, J.-H. Optical properties of silicon nanowires array fabricated by metal-assisted electroless etching. *SPIE Proc.* **2010**; p 77721C.

(22) Qin, Y.; Jiang, Y.; Zhao, L. Modulation of Agglomeration of Vertical Porous Silicon Nanowires and the Effect on Gas-Sensing Response. *Adv. Eng. Mater.* **2018**, *20*, 1700893.

(23) Zhao, Y.-P.; Fan, J.-G. Clusters of bundled nanorods in nanocarpet effect. *Appl. Phys. Lett.* **2006**, *88*, 103123.

(24) Mallavarapu, A.; Ajay, P.; Sreenivasan, S. Enabling ultrahigh-aspect-ratio silicon nanowires using precise experiments for detecting the onset of collapse. *Nano Lett.* **2020**, *20*, 7896−7905.

(25) Li, C.; Fobelets, K.; Tymieniecki, M. S.; Hamayun, M.; Durrani, Z. A. K.; Green, M. Bunch-Free Electroless-Etched Si Nanowire Array. *ECS Trans.* **2011**, *33*, 9−13.

(26) Choi, C.; Yoon, Y.; Hong, D.; Brammer, K. S.; Noh, K.; Oh, Y.; Oh, S.; Talke, F. E.; Jin, S. Strongly superhydrophobic silicon nanowires by supercritical CO2 drying. *Electron Mater. Lett.* **2010**, *6*, 59−64.
(27) Chun, D. W.; Kim, T. K.; Choi, D.; Caldwell, E.; Kim, Y. J.; Paik, J. C.; Jin, S.; Chen, R. Vertical Si nanowire arrays fabricated by magnetically guided metal-assisted chemical etching. *Nanotechnology* **2016**, *27*, 455302.
(28) Yoon, S.-S.; Khang, D.-Y. Switchable wettability of vertical Si nanowire array surface by simple contact-printing of siloxane oligomers and chemical washing. *J. Mater. Chem.* **2012**, *22*, 10625−10630.
(29) Hull, R. *Properties of Crystalline Silicon*; Institution of Electrical Engineers, 1999; p 1042.
(30) Li, H.; Ye, T.; Shi, L.; Xie, C. Fabrication of ultra-high aspect ratio silicon nanostructures by using Au metal assisted chemical etching. *J. Micromech. Microeng.* **2017**, *27*, 124002.
(31) Bockris, J. O.; Reddy, A. K. N.; Gamboa-Adelco, M. *Modern Electrochemistry 2A*; Springer, 2001; p 815.
(32) Okorn-Schmidt, H. F. Characterization of silicon surface preparation processes for advanced gate dielectrics. *IBM J. Res. Dev.* **1999**, *43*, 351−326.
(33) Shiu, S.-C.; Lin, S.-B.; Hung, S.-C.; Lin, C.-F. Influence of pre-surface treatment on the morphology of silicon nanowires fabricated by metal-assisted etching. *Appl. Surf. Sci.* **2011**, *257*, 1829−1834.
(34) Williams, K.; Muller, R. Etch rates for micromachining processing. *J. Microelectromech. Syst.* **1996**, *5*, 256−269.
(35) Morita, M.; Ohmi, T.; Hasegawa, E.; Kawakami, M.; Ohwada, M. Growth of native oxide on a silicon surface. *J. Appl. Phys.* **1990**, *68*, 1272−1281.
(36) Lohse, D.; Zhang, X. Surface nanobubbles and nanodroplets. *Rev. Mod. Phys.* **2015**, *87*, 981−1035.
(37) Zhang, X.; Chan, D. Y.; Wang, D.; Maeda, N. Stability of interfacial nanobubbles. *Langmuir* **2013**, *29*, 1017−1023.
(38) Backes, A.; Bittner, A.; Leitgeb, M.; Schmid, U. Influence of metallic catalyst and doping level on the metal assisted chemical etching of silicon. *Scr. Mater.* **2016**, *114*, 27−30.
(39) Elyamny, S.; Dimaggio, E.; Magagna, S.; Narducci, D.; Pennelli, G. High power thermoelectric generator based on vertical silicon nanowires. *Nano Lett.* **2020**, *20*, 4748−4753.

https://doi.org/10.1021/acsaelm.3c01014
ACS Appl. Electron. Mater. 2024, 6, 2917−2924